

Ozonation, photocatalysis and photocatalytic ozonation of diuron. Intermediates identification

Rafael R. Solís^{a,*}, F. Javier Rivas^a, Ana Martínez-Piernas^b, Ana Agüera^b

^aDepartment of Chemical Engineering and Physical Chemistry, University of Extremadura, Av. Elvas s/n, 06071 Badajoz, Spain

^bCIESOL, Joint Centre of the University of Almería-CIEMAT, La Cañada de San Urbano s/n, 04120 Almería, Spain

*Correspondence to: Rafael R. Solís, Departamento de Ingeniería Química y Química Física, Universidad de Extremadura, Avda. Elvas s/n, 06071, Badajoz (Spain). Email: rrodrig@unex.es, Phone: +34924289300, Fax: +34924289385

Abstract

Aqueous 3-(3,4-dichlorophenyl)-1,1-dimethylurea (diuron) has been oxidised by ozonation, photocatalysis and photocatalytic ozonation. Diuron degradation takes place via radical pathway through hydroxyl radicals in those systems involving ozone. Diuron elimination in photocatalytic ozonation is not enhanced if compared to single ozonation; however, TOC removal was significantly improved. Specifically, 80% TOC removal in 2 hours was reached in photocatalytic ozonation while single ozonation just led to 25% TOC reduction. Photocatalysis required 9 hours to reach 25% TOC reduction. Ten transformation by-products generated during the application of the three technologies were tentatively identified by liquid chromatography-quadrupole time-of-flight mass spectrometry (LC-QTOF-MS/MS). Single ozonation and photocatalytic ozonation led to the formation and complete elimination of all by-products. Low weight carboxylic acids evolution suggests that high TOC removal in photocatalytic ozonation is linked to its capacity to oxidise small oxygenated compounds and release of inorganic chloride and nitrate. Toxicity evolution to *Vibrio fischeri* in photocatalytic ozonation displayed an

increase in inhibition at the initial stages (>90% of inhibition), followed by a decrease of this parameter as the reaction progressed. The final treated sample shows a lower toxicity than the initial one (55% vs 20%).

Keywords: photocatalytic ozonation, diuron, transformation products, toxicity evolution

Highlights:

- $\cdot\text{OH}$ radical plays an important role in diuron photocatalytic ozonation (>99%).
- $\text{O}_3/\text{TiO}_2/\text{UVA}$ enhances TOC removal (83% synergism) if compared to simpler systems.
- By-products derive from $\cdot\text{OH}$ attack to the alkyl side chain and/or Cl substitution.
- $\text{O}_3/\text{TiO}_2/\text{UVA}$ is capable of mineralize small oxygenated species.
- Diuron toxicity to *Vibrio fischeri* shows a maximum at initial stages of oxidation.

1. INTRODUCTION

Intensive agriculture involves a high herbicide demand. The presence of these substances in the environment is alarmingly increasing all over the world. Since herbicides are usually persistent in soil and water, their presence supposes a potential harmful risk in natural ecosystems.

Water resources scarcity is an increasingly problem in many areas of the Earth. Recycling aqueous effluents by new treatment methods is a challenge for the scientific community. Although treating organic/inorganic pollutants by means of different technologies (usually biodegradation) is quite often viable, a variety of them, such as some pesticides, are recalcitrant to conventional biological treatments [1]. For this reason, more powerful oxidising technologies are required.

Organochlorides are some of the most popular and widely used pesticides. They derive from chlorinated hydrocarbons. The high physical and chemical stability favour their persistence and slow biodegradability in the environment. Diuron ($C_9H_{10}Cl_2N_2O$, 3-(3,4-dichlorophenyl)-1,1-dimethylurea) works by inhibiting the photosynthesis process. Diuron is an organochloride phenylurea herbicide commonly used as pre and post emergent herbicide of a huge variety of both, crop and non-crop areas. Diuron's use is currently approved in the European Union until 2018 [2]. This herbicide, whose presence has been reported in 70 % of 100 rives of 27 European Countries with a maximum concentration of $0.826 \mu\text{g L}^{-1}$ [3], appears to be moderately persistent and relatively immobile in water [4]. Moreover, because of its high toxicity, pollution due to this substance is considered as a real environmental hazard. This is evidenced by a recently launched European Directive which includes diuron in the list of priority pollutants in water treatment policy [5].

The harmful presence of phenylurea herbicides in aqueous environments has initiated a considerable research production, including ozone and advanced oxidation processes such as Fenton-based systems, photocatalysis and, ozone combined with UV radiation, catalysts or H₂O₂ [6]. Diuron ozonation has been reported in the literature as an effective technology [7]. Nevertheless, to the author's knowledge, individual diuron photocatalytic ozonation focused on the generated transformation products has not yet been reported.

Photocatalytic ozonation consists in the simultaneous application of ozone and photocatalysis. The process is presented as a promising chemical technology which reaches high mineralization rates. The combination of ozone in photocatalytic systems allows for a synergistic effect based on the high efficient electron trapping by ozone. Additionally higher amounts of hydroxyl radicals are generated if compared to photocatalysis in the presence of oxygen alone [8]. In spite of being an effective technology, separation of catalyst from the media and energy requirements must be considered at the time of scaling up. In any case, the synergistic effect frequently observed considerably reduces the costs if compared to photocatalysis or ozonation alone [9].

In the last years, photocatalytic efforts have been focused on developing more reliable and efficient photocatalysts which can take benefit of the solar spectrum more effectively [10]. Amongst the main proposed strategies, TiO₂ metal and non-metal doping [11], coupling of oxides to TiO₂ [12], photocatalysts alternative to TiO₂ and supported or easily removable solids [9, 13] can be listed. In this work, a lab manufactured N-doped titania has been used. N doping improvements on photoactivity and characterization of the solid have previously been studied in-depth in a mixture of three pyridine based herbicides, under photocatalysis and photocatalytic ozonation

processes [14]. Moreover, N-doping may be considered as a starting point in catalyst recovering due to the increase in particle size. A higher particle diameter, if compared to commercial formulas, makes easier the recovering process from the effluent. Ozonation and photocatalysis of diuron have been compared to photocatalytic ozonation under UVA radiation when required (maximum of emission at 365 nm).

The aim of the present work has been focused on the identification of the main transformation byproducts formed in photocatalytic ozonation and comparison to those generated under single ozonation or photocatalysis. Final oxidation organic acids evolution has also been monitored in order to explain TOC removal extents. Toxicity evolution to bacteria *Vibrio fischeri* has been studied for the three processes and compared to results of intermediates, organic acids released and TOC evolution.

2. MATERIALS AND METHODS

2.1. Chemicals

Analytical standard diuron was acquired from Sigma-Aldrich (>98%) and used as received in all experiments. HPLC-grade acetonitrile from VWR Chemicals was used in the HPLC system. Ionic chromatography solutions were prepared from Sigma-Aldrich reagents. Titanium isopropoxide (Sigma-Aldrich, >97%), trimethylamine (Panreac, 99.5%) and HCl (Fischer Scientific, 37%) were used in N doped titania photocatalyst synthesis. Potassium indigo trisulfonate, used in dissolved ozone monitoring, was purchased from Sigma-Aldrich (99%). Ultrapure water used in all trials was produced in a Mili-Q® academic (Millipore) system.

Chemicals for mobile phase in LC-QTOF-MS analysis (water, >99.9% and acetonitrile, >99.9%) were LC-MS CROMASOLV® from Fluka. Formic acid was used (98%, LC-MS from Fluka) to acidify water.

2.2. Experimental setup and procedure

Photoreaction installation was equipped with a 1.0 L volume cylindrical reactor made of borosilicate glass. The reactor was placed into a cylinder pipe (54 cm of height and 31cm of external diameter) equipped with four black light lamps of 41cm of length (LAMP15TBL HQPOWER™ 15 W emitting in the range 350-400 nm, maximum at 365 nm). The inner surface was covered with aluminum foil in order to enhance photons reflection. UVA photon flow entering the reaction system was calculated in a previous work by means of ferrioxalate actinometry. Values of 1.77, 3.26, 5.13 and $6.86 \cdot 10^{-5}$ Einstein $\text{min}^{-1} \text{L}^{-1}$ when 1, 2, 3 and 4 lamps, were reported [15]. Additionally, when the aluminium foil covering the internal walls of the installation was substituted by a black surface, the intensity (4 lamps switched on) decreased to $3.60 \cdot 10^{-5}$ Einstein $\text{min}^{-1} \text{L}^{-1}$.

In a typical experiment, 30 L h^{-1} gas flow rate of oxygen, or an oxygen-ozone mixture, was fed to the photoreactor system through a stainless steel diffuser. Solid photocatalyst was added 30 min before starting the reaction, in order to reach the possible adsorption equilibria onto its surface. Samples at different times were extracted and filtered by means of Millex-HA filters (Millipore, 0.45 μm) before analysis.

Ozone was continuously generated by electrical discharges of pure oxygen in a Sander Laboratory Ozone Generator. An Anseros Ozomat ozone analyser, the measurement based on 254 nm absorbance, was used to monitor ozone gas phase concentration.

2.3. Photocatalyst synthesis

N doped titania photocatalyst was prepared applying a sol-gel method followed by thermal treatment and calcination according to literature and previous works [16, 14]. Briefly, 12 mL of titanium (IV) isopropoxide were dissolved in 100 mL of ethanol. Next, 9 mL of trimethylamine was added. Afterwards, titania was precipitated using 100 mL of HCl 0.1 M. The suspension was thermally treated at 80°C for 12 hours. The final

residue was dried overnight at 100°C and calcined at 500°C for 4 hours (initial ramp of 10°C min⁻¹)

2.4. Analytical methods

Diuron was analysed by an Agilent 1100 (Hewlett-Packard) high performance liquid chromatography with UV detection (HPLC-UV). The column used was a Kromasil 100 5C18 (5µm, 2.1x150 mm). 0.1% H₃PO₄ acidified water (A) and acetonitrile (B) were the mobile phases used. An elution gradient from 50% to 65% of B in 6 min was applied. UV detection was conducted at 243 nm.

Liquid chromatography coupled to a quadrupole time-of-flight mass spectrometer (LC-QqTOF-MS) was used to identify and monitor transformation products generated in single ozonation, photocatalytic oxidation and photocatalytic ozonation processes. Chromatographic separation was carried out in an Agilent 1260 Infinity system equipped with a Poroshell 120 EC-C18 (2.7 µm, 4.6x50 mm) column. Pure MiliQ water (phase A) or acidified water with 0.1% formic acid (for negative and positive ionization modes, respectively), and acetonitrile (phase B) were used as mobile phases. Elution gradient at 0.4 mL min⁻¹ flow rate went from 10% A (1 min) to 100% B in 10 min, and kept thereafter for 5 min before returning to initial conditions. Injection was completed with 10 µL. HPLC system was connected to a hybrid quadrupole time-of-flight mass spectrometer TRIPLE TOF 5600+ system (AB Sciex) with an electrospray interface (ESI). Both ESI (+) and ESI (-) modes were considered for unknown transformations products (TPs) identification. The equipment worked via TOF MS survey scan followed by four IDA (Information Dependent Acquisition) TOF MS/MS scans. Alternatively to IDA mode, other tools like 'mass defect filters' and 'include list' for potential candidates were used in order to focus and shorten TPs identification during the acquisition process. Besides, for low intensity TPs, the SWATH® tool was considered

to obtain MS/MS fragmentation patterns. Scanned mass range was from $m/z=50$ to 800 Da, either in TOF or MS/MS experiments. An accumulation time of 100 ms was used in each scan. IDA criteria considered dynamic background subtraction. Collision energy of 30 eV with a ± 10 eV spread was used in MS/MS fragmentation. Diverse AB SCIEX software (Analyst TF 1.5, PeakView™ 2.2 and MasterView 1.1) was used to record and process LC-QTOF-MS data. MasterView processing was also enhanced with potential candidates lists based on computational (*in-silico*) prediction tools like University of Minnesota Pathway Prediction System and PathPred [17].

Ionic short chain organic and inorganic anions were monitored by ionic chromatography using a Metrohm 881 Compact Pro ionic connected to MagIC NET™ software.

Total organic carbon (TOC) was determined by a Shimadzu TOC 5000A analyser.

Aqueous dissolved ozone was measured by Bader and Hoigné method [18], the analysis is based on 5,5,7-indigo-trisulfonate decolouration, spectrophotometrically determined at 600 nm.

2.5. Ecotoxicity assays

Toxicity evolution was evaluated by means of the bioluminescence bacterium *Vibrio fischeri* inhibition to reaction samples. Microtox 500 was used at room temperature to quantify light emitting decay when exposed to reaction samples extracted at different oxidation times. Luminescence decay was recorded at different exposure times (5, 15 and 30 min) and inhibition percentages were calculated.

3. RESULTS

3.1. Efficiency of ozonation, photocatalysis and photocatalytic ozonation

Some preliminary experimental series were conducted to assess the efficacy of different oxidation systems on both, diuron and TOC removal. Additionally, the effect of

different catalysts (doped, undoped and commercial TiO₂) was also investigated. Experimental conditions such as catalyst load and ozone dose have been chosen according to previous literature [19]. Figure 1 shows the results obtained.

Figure 1 reveals some interesting aspects. Hence, no appreciable difference in diuron conversion was experienced in runs conducted in the presence of ozone. Single ozonation, catalytic ozonation and photocatalytic ozonation led to similar diuron depletion rates. However, contrarily to the first thought, in these systems diuron (and likely TOC) is mainly removed by the action of hydroxyl radicals generated after ozone decomposition. Some simple calculations could corroborate the previous hypothesis.

If the heterogeneous reaction develops in the slow regime, the following rate expression can be applied:

$$-\frac{dC_{\text{DIU}}}{dt} = k_{\text{O}_3} C_{\text{DIU}} C_{\text{O}_3} + k_{\bullet\text{OH}} C_{\text{DIU}} C_{\bullet\text{OH}} \quad (1)$$

Where k_{O_3} and $k_{\bullet\text{OH}}$ are the second order rate constants of the reactions between diuron and ozone and hydroxyl radicals, respectively. The Hatta number was thereafter calculated to estimate the regime of the reaction. Hatta number (Ha) is defined as:

$$\text{Ha} = \frac{\sqrt{C_{\text{DIU}} k_{\text{O}_3} D_{\text{O}_3}}}{k_L} \quad (2)$$

D_{O_3} stands for ozone diffusivity in water and k_L is the individual mass transfer coefficient in the liquid phase. Values used to calculate Ha were $D_{\text{O}_3} = 1.7 \cdot 10^{-9} \text{ m}^2 \text{ s}^{-1}$ [20] and $k_L = 5 \cdot 10^{-5} \text{ m s}^{-1}$, typical of bubble contactors. When $\text{Ha} < 0.03$ slow regime kinetic is developed. If only the reaction of diuron with molecular ozone took place, which can experimentally be tested adding a hydroxyl radical inhibitor, such as tert-butyl alcohol, equation 1 would reduce to:

$$-\frac{dC_{\text{DIU}}}{dt} = k_{\text{O}_3} C_{\text{DIU}} C_{\text{O}_3, \text{d}} \quad (3)$$

Since ozone concentration was experimentally measured, equation 3 could be numerically solved by applying the simple Euler method:

$$C_{\text{DIU}}^{t+1} = C_{\text{DIU}}^t - (k_{\text{O}_3} C_{\text{DIU}}^t C_{\text{O}_3, \text{d}}^t) \Delta t \quad (4)$$

In the previous expression, ozone concentration was adjusted to a third order polynomial leading to:

$$C_{\text{DIU}}^{t+1} = C_{\text{DIU}}^t - (k_{\text{O}_3} C_{\text{DIU}}^t [at^3 + bt^2 + ct + d]) \Delta t \quad (5)$$

Figure 2 shows the experimental evolution of diuron in absence and presence of tert-butyl alcohol. A value of $k_{\text{O}_3} = 19.2 \pm 1.1 \text{ M}^{-1}\text{s}^{-1}$ ($R^2 > 0.99$) was obtained by considering the ozonation in presence of tert-butyl alcohol, where Ha value was always below 0.03. Other authors have reported similar kinetic rate constant values, $14.7 \text{ M}^{-1}\text{s}^{-1}$ [21] and $16.5 \text{ M}^{-1}\text{s}^{-1}$ [22], evaluated under competition kinetic methods.

As observed from Figure 2, the radical pathway of diuron oxidation plays an important role under the operating conditions used in this study.

Moreover, since diuron conversion in the absence of tert butanol does not depend on initial concentration, Figure 2 suggests that the concentration curves obey first order kinetics. First order kinetics can be obtained provided that $k_{\text{O}_3} C_{\text{DIU}} C_{\text{O}_3} \ll k_{\bullet\text{OH}} C_{\text{DIU}} C_{\bullet\text{OH}}$ and $C_{\bullet\text{OH}}$ is kept constant during the process, i.e. quasi steady state conditions in hydroxyl radicals concentration applies. Accordingly, equation 1 was now solved optimizing the $C_{\bullet\text{OH}}$ to minimize the differences between experimental and calculated DIU depletion profiles. A steady state hydroxyl radical concentration of $7.1 \cdot 10^{-13} \text{ M}$, assuming $k_{\bullet\text{OH}} = 6.6 \cdot 10^9 \text{ M}^{-1} \text{ s}^{-1}$ [23], was found to acceptably model the process. This

result allows for elucidating the percentage of indirect diuron removal due to hydroxyl radicals as the ratio:

$$\eta_{\cdot\text{OH}} = \frac{k_{\cdot\text{OH}} C_{\cdot\text{OH}}}{k_{\text{O}_3} C_{\text{O}_3} + k_{\cdot\text{OH}} C_{\cdot\text{OH}}} \times 100 \quad (6)$$

This ratio had a minimum around 99% when ozone concentration reached its maximum but DIU conversion was above 99% (see figure 2) which is similar and consistent with previous ozonation works [7].

As DIU was mainly eliminated by hydroxyl radicals, photocatalytic ozonation would have been expected to enhance the DIU depletion rate; however, this was not the case. Previous results indicate that hydroxyl radicals generated in the presence of ozone are sufficient to degrade diuron and additional active species from the photocatalytic system do not play a significant role in diuron conversion. Nevertheless, substantial differences were experienced when analysing TOC results. Figure 1 shows a poor 25% mineralization when O₃ or O₃/N-TiO₂ was applied for 2 hours. Photocatalysis could achieve similar results only after 9 hours. Mineralization, however, reached an outstanding (if compared to the rest of systems) 80% after 120 minutes when photocatalytic ozonation was used. A synergistic effect could therefore be obtained when simultaneously applying the photocatalysis in the presence of ozone. Ozone might improve photocatalytic systems by trapping photo-generated electrons, avoiding, therefore, the undesirable hole-electron recombination. Additionally, after electron trapping, more active species (mainly radicals) are generated [8]. The extent of synergism can be calculated from:

$$\Lambda_{\text{Synergisms}} = \frac{k_{\text{PhotCat-O}_3} - [k_{\text{Ozonation}} + k_{\text{PhotCat}}]}{k_{\text{PhotCat-O}_3}} \times 100 \quad (7)$$

Where $k_{\text{PhotCat-O}_3}$, $k_{\text{Ozonation}}$ and k_{PhotCat} are empirical pseudofirst order rate constants corresponding to photocatalytic ozonation, single ozonation and photocatalysis, respectively. TOC removal pseudo first order rate constants values obtained from Figure 1 were, when N-TiO₂ was applied, $1.66 \cdot 10^{-2} \text{ min}^{-1}$ ($R^2 = 0.997$), $1.90 \cdot 10^{-3} \text{ min}^{-1}$ ($R^2 = 0.995$) and $0.8 \cdot 10^{-3} \text{ min}^{-1}$ ($R^2 = 0.992$), for $k_{\text{PhotCat-O}_3}$, $k_{\text{Ozonation}}$ and k_{PhotCat} respectively. Synergism percentage was calculated to be 83.7%.

Moreover, Figure 1 shows that N doping of TiO₂ improves photoactivity in the photocatalytic ozonation process. Although Figure 1 shows no significant differences in diuron removal for undoped and doped catalyst, N-TiO₂ led to higher mineralization rates than undoped TiO₂. Undoped titania achieved 40% TOC reduction after 180 min while N doped TiO₂ led to 80% under the same operating conditions. Physical properties of solids and its photoactivity behaviour have previously been discussed [14]. Commercial P25 also exhibits 80% of mineralization.

After assessing the efficiency of the different systems under study, in the next stage an attempt was conducted to identify some of the most important transformation products (TPs) generated during their application.

3.2. Identification of TPs by LC-QTOF-MS/MS and ionic chromatography

In this work, 10 compounds have been tentatively identified by LC-QTOF-MS/MS. Table 1 summarizes, organized in increasing experimental accurate mass value, some of their characteristics such as generating system, retention time and elemental composition of the protonated/deprotonated ions and their fragment ions, obtained by ESI(+) or ESI(-) and Rings plus Double Bonds Equivalent (RDBE).

Diuron and some of their TPs were identified in both ESI(-) and ESI(+) modes. From the $[\text{M-H}]^-$ ion two fragments were obtained corresponding to the loss of the $-\text{NH}(\text{CH}_3)_2$ group and further chloride release from the aromatic ring. From the $[\text{M+H}]^+$ three

fragments were detected, again the loss of the $-\text{NH}(\text{CH}_3)_2$ group and the two moieties resulting from breakage of the $-\text{CO}-\text{NH}(\text{CH}_3)_2$ side chain. This MS/MS fragmentation pattern may be useful to interpret where the initial molecule has easiness to be oxidized since this are the more likely bounds to be broken by oxidation processes [22].

The first transformation product TP1 was given an ion formula $[\text{C}_9\text{H}_9\text{Cl}_2\text{N}_2\text{O}_3]^-$. Figure 4 shows the product ion spectra and tentative fragment ion structures of some TPs found in this investigation,. This molecule could be the result of two hydrogen abstractions by hydroxyl radicals present in the three investigated systems. Hydroxylation of diuron has been reported to occur in photocatalytic systems both in the aromatic ring and $-\text{CH}_3$ groups [24, 25]. However, fragmentation of the precursor led to the loss of a $-\text{CH}(\text{OH})_2$ group and further release of the $-\text{CO}-\text{NHCH}_3-\text{CH}(\text{OH})_2$ moiety, suggesting that hydroxyl attack has occurred in one of the external methyl chains. The proposed structure of this transformation product has also been reported in the photo Fenton treatment of a mixture of diuron and linuron [26]. Attack of hydroxyl radicals to N-methylated derivatives of formamide and acetamide has been reported to occur by abstraction of hydrogen from the methyl group [27].

TP2 presents an ion formula $[\text{C}_8\text{H}_8\text{Cl}_2\text{N}_2\text{O}_3]^+$ obtained in ESI(+) mode. It would result from demethylation of TP1 and further release of a molecule of formaldehyde. Fragmentation of TP2 suggests the presence of the dichlorophenyl structure (loss of the $\text{CO}-\text{NH}-\text{CH}(\text{OH})_2$ group). The proposed formula would be 3-(3,4-dichlorofenil)-1,1-dihydroxy urea. This compound has also been proposed as an intermediate in the photo Fenton process [26]. In this investigation TP2 was only detected when single ozonation was used. TP2 is also likely to be generated in the photocatalytic ozonation but it must be instantaneously removed from the reaction media, so it could not be detected.

TP3 was identified in those systems using radiation. The ion formula of this compound, $[C_9H_{11}Cl_2N_2O_2]^+$, maintains the same number of carbons than the parent herbicide. Fragmentation of the precursor leads to the detection of an m/z moiety corresponding to the dichloroaniline ion. Accordingly, loss of a $-CO-N(CH_3)CH_2OH$ group is suggested. TP3 formation is previous to TP1, since hydroxylation of methyl group takes place in two steps. The presence of this structure in the photo Fenton and photocatalytic systems has been reported [24, 26, 28].

TP4 led to 4 fragments in ESI(-) and 2 fragments in ESI(+) modes. The precursor was tentatively assigned in ESI (-) as $[C_9H_7Cl_2N_2O_2]^-$ (or $[C_9H_9Cl_2N_2O_2]^+$ in ESI(+) mode). Fragments in ESI(-) mode indicated losses of $-CO$, $-N(CH_3)CO$ and $-CON(CH_3)CO$ (see Figure 3). TP4 is the main byproduct of diuron oxidation detected in photocatalytic [24, 28], photoFenton [26, 28] and ozonation [29, 30] systems.

TP5 was identified in ESI(+) and ESI(-) modes, in both cases fragmentation led to the release of the $-CONHCH_3$ group. The proposed structure of this transformation product is likely to be the result of diuron demethylation, already reported in all the cited works dealing with identification of byproducts of diuron.

TP6 was the only transformation product suggesting the hydroxylation of the aromatic ring by substitution of one of the chloride groups in the parent herbicide. This hypothesis is substantiated by the analysis of the fragments generated from the precursor (see Figure 3). Hence, in ESI(-) mode the precursor $[C_9H_{10}ClN_2O_2]^-$ exhibits the typical loss of the $-NH(CH_3)_2$ group, followed by losses of the $-CO$ group or the HCl neutral loss. The absence of the ion 159.9715 ($C_6H_4Cl_2N^+$) found in the rest of TPs that still maintain the chloroaniline structure, which also indicates the breakage of the ring.

TP7 was only detected in the ozonation process, being the unique transformation product resulting from the aromatic ring opening. Fragmentation of TP7 leads to the release of H₂O, -COOH and -CO-N(CH₃)₂ groups. The lower retention time and RDBE value compared to the rest of precursors is consistent with the increased polarity of the proposed structure confirming the suggested structure. No bibliographic reference could be found for this compound. The proposed structure indicates a high degree of oxidation with two acidic groups located in the opened ring (see Table 1). It is noteworthy to say that the side chain bounded to the aromatic ring in the original diuron molecule is kept unchanged in TP7, suggesting that multiple hydroxyl attack to the aromatic ring has previously occurred. This is substantiated by a high release of Cl⁻ during ozonation process (see below in Figure 6).

TP8 was only detected in the photocatalytic systems. Moreover, TP8 (together with TP4) accumulates in the reaction media after 540 min of photocatalysis treatment showing a high intensity. TP8 involves the release of one molecule of dimethylamine (or *N,N*-dimethylhydroxyamine) from diuron and further formation of an oxazole like ring. No reference has reported the formation of this compound; however two ring transformation products have been suggested elsewhere [31].

TP9 structure is the result of the release of the dimethylamine group (or *N,N*-dimethylhydroxyamine) from diuron. Fragmentation of TP9 includes the loss of -CHO in one of the fragments and the two -Cl of the aromatic ring in the other analysed fragment (Figure 3).

Finally, TP10 suggests the formation of dichloroaniline, the typical end product in all kind of incomplete diuron mineralization systems.

Based on the structures found in this work and results presented in literature [24, 27, 28], Figure 4 summarizes the proposed mechanism pathway degradation by $\bullet\text{OH}$ radical attack. Since direct ozonation is negligible if compared to $\bullet\text{OH}$ radical pathway, TPs formation is assumed to be the consequence of hydroxyl radicals reactions. Two different routes have been considered, the attack and oxidation of the alkyl side chain and the substitution of chlorine by OH groups. However, other authors include the $\bullet\text{OH}$ attack to aromatic rings and simultaneous substitution of chlorine by $\bullet\text{OH}$, oxidation of alkyl chain and $\bullet\text{OH}$ attack to aromatic rings [28]; reactions that have not been considered in this work.

Figure 5 shows the evolution of normalized intensity of TPs related to maximum intensity of diuron at time zero. Normalized intensity percentage is not necessarily proportional to concentration in the same proportion for all compounds, i.e. peak intensity highly depends on analytical operating conditions and easiness of ionization of the TP. However, this parameter could give an approximated idea of the amount of TP generated and its evolution with time. Accordingly, from Figure 5 some hypothesis can be derived. Hence, in the ozonation process, based on peak intensity, TP2 and TP4 are the transformation products showing a higher transient concentration in the media with a maximum located in the range 5-7.5 min and 2.5-5 min for TP2 and TP4, respectively.

Photocatalytic ozonation is characterized by the apparent high selectivity of the process towards TP4 formation, achieving a peak intensity of roughly 45% of the initial diuron intensity. Also, if compared to the ozonation process, maximum in concentration for some TPs are shifted from the range 2.5-7.5 min to values above 20 min. Thus, TP1, TP9 and TP10 show increasing intensities from 0 to 20 min.

The photocatalysis was the least efficient system. Diuron and TPs were detected even after 540 min of reaction. TP8 and TP4 were the TPs presenting a higher intensity. The first one was only detected in this system.

Figure 6 displays the evolution of some typical low weight organic acids that accumulate in the media after applying advanced oxidation systems. Also nitrate and chloride profiles are shown. As observed, chloride appears in the three systems almost from the beginning, suggesting that hydroxylation of diuron aromatic ring immediately takes place coinciding with the hydroxyl attack to the chain attached. Also it has to be pointed out that, when ozone is present, chloride concentration linearly increases from the initial state until diuron has disappeared, thereafter a second slower period of chloride accumulation occurs due to chloride release from intermediates. Nitrate follows a similar pattern in the ozonation process although a short lag period previous to its detection was found. This lag period was more evident in the photocatalytic ozonation. In this process nitrates were not detected until diuron was completely depleted. Thereafter nitrate concentration linearly increased up to the values predicted from the initial diuron concentration. The higher mineralization capacity of the photocatalytic ozonation, if it is compared to single ozonation, is the capacity of oxidising small oxygenated molecules. This fact is patent after observing the concentration profiles of formic acid in both systems. Formic acid reached a value of 1.16 ppm after 180 min of ozonation, followed by a clear upward trend, while this compound presented a maximum of around 1.03 ppm in photocatalytic ozonation at 30 min sharply decreasing its concentration to 0.05 ppm at 120 min. In opposition to single ozonation, photocatalytic ozonation is capable of removing formic acid. Finally, it should be mentioned the absence of nitrates in the photocatalytic process which agrees with the fact that nitrogen derivatives of diuron are still present in solution.

3.3. Evolution of toxicity to *Vibrio fischeri*

Toxicity of TPs towards *V. fischeri* was assessed at different times of exposure in samples taken along the reaction period in single ozonation, photocatalysis and photocatalytic ozonation runs. Figure 7 depicts the inhibition percentage as a function of time. This figure shows diverse trends when using different systems. With the exception of photocatalysis, a slight increase in toxicity at the initial stages of the oxidation followed by a decrease in toxicity as the reaction proceeds is observed. This tendency is related to a higher toxicity from initial intermediates. As low weight oxygenated species are being formed, toxicity tends to be reduced. In relation to diuron toxicity, Gatidou and co-workers [32] reports an EC₅₀ value of 9.2 mg L⁻¹ after 30 min of exposition to *V. fischeri*.

Although ozonation and photocatalytic ozonation display similar toxicity responses with a maximum (> 90% inhibition at 30 min of exposure) followed by decrease; some slight differences could be extracted. Hence, photocatalytic ozonation exhibits lower inhibition values at the final stage of the process, when small organic acids and TOC are removed from the media. After 3 hour of treatment ozonation decreased the inhibition percentage to 55% while photocatalytic ozonation reduced it to 20%. The maximum inhibition reached might be due to the higher toxicity of intermediates compared to diuron, especially TP10 (3,4-dichloroaniline) which is the most toxic transformation product [33, 34]. Moreover, photocatalytic ozonation clearly reaches its maximum in toxicity at 5 minutes, while ozonation requires 15-20 min. This delay supports the idea that maximum of toxicity matches maximum of TPs formation in each oxidation technology, discussed previously.

In the case of photocatalysis, the inhibition profile steadily increases through the process because of the incomplete oxidation of intermediates. According to Figure 5,

photocatalysis is the technology displaying the highest values of TPs intensity. This explains why after 9 hours of treatment inhibition percentage reaches 85% (30 min of exposure).

4. CONCLUSIONS

Diuron has a low rate constant towards molecular ozone, accordingly, oxidation processes involving ozone take place via hydroxyl radical, this latter pathway supposes above 99%. Photocatalytic ozonation does not significantly improve parent compound removal. However, high TOC removal rates are reached by this system, showing an outstanding 83% of synergism in TOC removal if compared to single ozonation and photocatalysis.

Transformation products derived from ozonation, photocatalysis and photocatalytic ozonation are quite similar since the radical pathway plays an important role in the three systems. In processes in the presence of ozone, TPs maximum formation were observed once diuron was abated, afterwards they were utterly removed. Photocatalytic ozonation displayed high selectivity to TP4 formation (*N*-[(3,4-dichlorophenyl)carbamoyl]-*N*-methylformamide).

High mineralization rates linked to photocatalytic ozonation are due to the high capacity of oxidising small oxygenated organics. Chloride evolution suggests that hydroxylation of diuron takes place coinciding with hydroxyl radical attack. Inorganic nitrogen was not displayed until diuron was completely depleted.

Toxicity evolution to *V. fischeri* during photocatalytic ozonation showed an increase at the initial oxidation stage (> 90%) decreasing thereafter as the reaction progresses. Ozonation displayed a lower ability to decrease the inhibition percentage after reaching the maximum in toxicity. Photocatalysis gradually increased the toxicity to the bacteria.

Photocatalytic ozonation has a powerful capacity of generating radicals making possible the oxidation of organic pollutants, with high environmental concern. This is the origin of the observed higher mineralization rate if compared to single ozonation or photocatalysis.

Acknowledgements

Authors thank economic support received from Gobierno de Extremadura and CICYT of Spain through Projects GRU10012 and CTQ2012-35789-C02-01, respectively. Mr. Rafael Rodríguez Solís also thanks Gobierno de Extremadura, Consejería de Empleo, Empresa e Innovación, and FSE Funds for his Ph.D. grant (PD12058).

References

- [1] M. Gavriescu, Fate of Pesticides in the environment and its bioremediation, *Eng. Life Sci.* 5 (2005) 497-526.
- [2] Commission Directive 2008/91/CE of 29 September 2008 amending Council Directive 91/414/EEC to include diuron as active substance, *Official Journal of the European Union* 262 (2008) 31-32.
- [3] R. Loos, B.M. Gawlik, G. Locore, E. Rimaviute, S. Contini, G. Bidoglio, EU-wide survey of polar organic persistent pollutants in European river water, *Environ. Pollut.* 157 (2009) 561-568.
- [4] Pesticide Properties Database. University of Hertfordshire, UK. <http://sitem.herts.ac.uk/aeru/ppdb/en/index.htm>, 2016 (last accessed 01.02.16).
- [5] EU Directive 2013/39/EU of the European Parliament and The Council of 12 August 2013 amending Directives 2000/60/EC and 2008/105/EC as regards priority substances in the field of water policy, *Official Journal of the European Union* 226 (2013) 1-17.

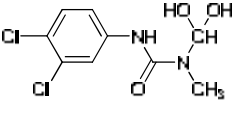
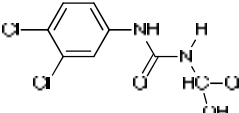
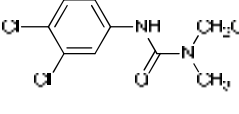
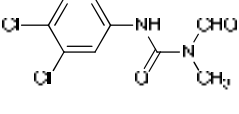
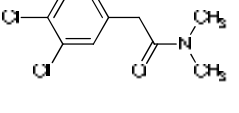


- [6] A.R. Ribeiro, O.C. Nunes, M.F.R. Pereira, A.M.T. Silva, An overview on the advanced oxidation processes applied for the treatment of water pollutants defined in the recently launched Directive 2013/39/EU, *Environ. Int.* 75 (2015) 33-51.
- [7] R. Rosal, A. Rodríguez, J.A. Perdígón-Melón, A. Petre, E. García-Calvo, M.J. Gómez, A. Agüera, A.R. Fernández-Alba, Occurrence of emerging pollutants in urban wastewater and their removal through biological treatment followed by ozonation, *Water Res.* 44 (2006) 578-588.
- [8] T.E. Agustina, H.M. Ang, V.K. Vareek, A review of synergistic effect of photocatalysis and ozonation on wastewater treatment, *J. Photochem. Photobiol. C: Photochem. Rev.* 6 (2005) 264-273.
- [9] J. Xiao, Y. Xie, H. Cao, Organic pollutants removal in wastewater by heterogeneous photocatalytic ozonation, *Chemosphere* 121 (2015) 1-17.
- [10] S. Malato, P. Fernández-Ibáñez, M. Maldonado, J. Blanco, W. Gernjak, Decontamination and disinfection of water by solar photocatalysis: Recent overview and trends, *Catal. Today* 147 (2009) 1-59.
- [11] M. Peláez N.T. Nolan, S.C. Pillai, M.K. Seery, P. Falaras, A.G. Kontos, P.S.M. Dunlop, J.W.J. Hamilton, J.A. Byrne, K. O'Shea, M.H. Entezari, D.D. Dionysiou, A review on the visible light active titanium dioxide photocatalysts for environmental applications, *Appl. Catal. B: Environ.* 125 (2012) 331-349.
- [12] R. Daghrir, P. Drogui, D. Rober, Modified TiO₂ for environmental photocatalytic applications: a review, *Ind. Eng. Chem. Res.* 52 (2013) 2581-3599.
- [13] M.D. Hernández-Alonso, F. Fresno, S. Suárez, J.M. Coronado. Development of alternative photocatalysts to TiO₂: Challenges and opportunities, *Energy Environ. Sci.* 2 (2009) 1231-1257.

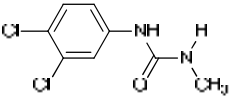
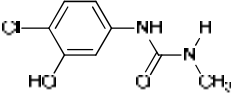
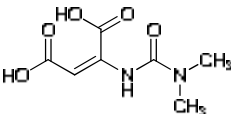
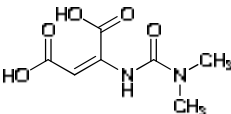
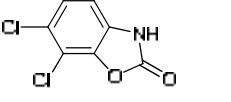
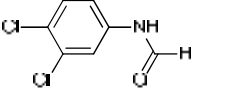
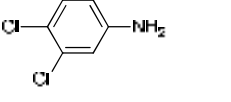
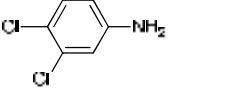
- [14] R.R. Solís, F.J. Rivas, O. Gimeno, O. and J.L. Pérez-Bote, Photocatalytic ozonation of pyridine-based herbicides by N-doped titania, *J. Chem. Technol. Biotechnol.* (2015) DOI: 10.1002/jctb.4791.
- [15] J. Rivas, R.R. Solis, O. Gimeno, J. Sagasti, Photocatalytic elimination of aqueous 2-methyl-4-chlorophenoxyacetic acid in the presence of commercial and nitrogen-doped TiO₂, *Int. J. Environ. Sci. Technol.* 12 (2015) 513-526.
- [16] J. Senthilnathan, L. Philip, Photocatalytic degradation of lindane under UV and visible light using N-doped TiO₂, *Chem. Eng. J.* 161 (2010) 83-92.
- [17] A.A. Bletsou, J. Jeon, J. Hollender, E. Archontaki, N.S. Thomaidis, Targeted and non-targeted liquid chromatography-mass spectrometric workflows for identification of transformation products of emerging pollutants in the aquatic environment, *Trends Anal. Chem.* 66 (2015) 32–44.
- [18] H. Bader, J. Hoigné, Determination of ozone in water by the indigo method, *Water Res.* 15 (1981) 449-456.
- [19] R.R. Solís, F.J. Rivas, O. Gimeno, J.L. Pérez-Bote, Photocatalytic ozonation of clopyralid, picloram and triclopyr. Kinetics, toxicity and influence of operational parameters, *J. Chem. Technol. Biotechnol.* 91 (2016) 51-58.
- [20] P.N. Johnson, R.A. Davis, Diffusivity of Ozone in Water, *J. Chem. Eng. Data* 41 (1996) 1485–1487.
- [21] J. de Laat, P. Maouala-Makata, M. Dore, Constantes cinétiques de réaction de l’ozone moléculaire et des radicaux hydroxyles sur quelques phenyl-urees et acetamides (Rate constants of ozone and hydroxyl radicals with several phenyl-ureas and acetamides), *Environ. Technol.* 17 (1996) 707-716.

- [22] F.J. Benítez, F.J. Real, J.L. Acero, C. García, Kinetics of the transformation of phenyl-urea herbicides during ozonation of natural waters: Rate constants and model predictions, *Water Res.* 41 (2007) 4073-4084.
- [23] A. Agüera, M.M. Gómez Ramos, A.R. Fernández-Alba, Chemical Evaluation of Water Treatment Processes by LC–(Q)TOF-MS: Identification of Transformation Products, in: A.R. Fernández-Alba (Ed.), *TOF-MS within Food and Environmental Analysis*, *Comp. Anal. Chem.*, 2012, pp. 61-109.
- [24] M.C. López, M.I. Fernández, S. Rodríguez, J.A. Santaballa, S. Steenken, E. Vulliet, Mechanisms of Direct and TiO₂-Photocatalysed UV Degradation of Phenylurea Herbicides, *ChemPhysChem* 6 (2005) 2064-2074.
- [25] M. Carrier, M. Besson, C. Guillard, E. Gonze, Removal of herbicide diuron and thermal degradation products under Catalytic Wet Air Oxidation conditions, *Appl. Catal. B: Environ.* 91 (2009) 275-283.
- [26] M.J. Farré, S. Brosillon, X. Domenech, Evaluation of the intermediates generated during the degradation of Diuron and Linuron herbicides by the photo-Fenton reaction, *J. Peral, J. Photochem. Photobiol. A: Chem.* 189 (2007) 364-373.
- [27] E. Hayon, T. Ibata, N.N. Lichtin, M. Simic, Sites of attack of hydroxyl radicals on amides in aqueous solution. II. Effects of branching alpha to carbonyl and to nitrogen, *J. Am. Chem. Soc.* 93 (1971) 5388–5394.
- [28] S. Malato, J. Cáceres, A.R. Fernández-Alba, L. Piedra, M.D. Hernando, A. Agüera, Photocatalytic Treatment of Diuron by Solar Photocatalysis: Evaluation of Main Intermediates and Toxicity, *J. Vial, Environ. Sci. Technol.* 37 (2003) 2516-2524.
- [29] J. Feng, Z. Zheng, J. Luan, J. Zhang, L. Wang, Degradation of diuron in aqueous solution by ozonation, *J. Environ. Sci. Health Part B* 43 (2008) 576-587.

- [30] R.M. Ramírez-Zamora, R. Seux, Identification du diuron et identification de quelques sous produits de la reaction, Rev. Sci. de l'eau 12 (1999) 545-560.
- [31] W. Pradittakan, E. Sadudeewong, K. Apichatsanee1, A.S. Vangnai, V. Pavarajarn, Comparative study of photocatalytic degradation of diuron on titanium dioxide and zinc oxide nanoparticles, in proceedings of Chemeca 2011: Engineering a better world, Sydney (2011) (ISBN: 978-0858259225).
- [32] G. Gatidou, A.S. Stasinakis, E.I. Iatrou, Assessing single and joint toxicity of three phenylurea herbicides using *Lemna minor* and *Vibrio fischeri* bioassays, Chemosphere 119 (2015) S69-S74.
- [33] J.L. Bonnet, F. Bonnemoy, M. Dusser, J. Bohatier, Assessment of the potential toxicity of herbicides and their degradation products to nontarget cells using two microorganisms, the bacteria *Vibrio fischeri* and the ciliate *Tetrahymena pyriformis*, Environ Toxicol. 22 (2007) 78-91.
- [34] C. Tixier, P. Bogaerts, M. Sancelme, F. Bonnemoy, L. Twagilimana, A. Cuer, J. Bohatier, H. Veschambre, Fungal biodegradation of a phenylurea herbicide, diuron: structure and toxicity of metabolites, Pest. Manag. Sci. 56 (2000) 455-462.

Table 1. Proposed intermediates found by LC-QTOF-MS/MS after diuron oxidation by ozone, photocatalysis and photocatalytic ozonation

TP	Oxidation process	Rt (min)	Experimental Exact Mass (error, ppm)	Ion formula, [M+H] ⁺	Ion formula, [M-H] ⁻	RD BE
TP1 	O ₂ /UVA/CAT		262.9996 (2.19)		C ₉ H ₉ Cl ₂ N ₂ O ₃ ⁻	5.0
	O ₃	9.20	216.9940 (2.10)		C ₈ H ₇ Cl ₂ N ₂ O ⁻	5.0
	O ₃ /UVA/CAT		159.9726 (3.25)		C ₆ H ₄ Cl ₂ N ⁻	4.0
TP2 	O ₃	10.64	250.9985 (-2.1)	C ₈ H ₈ Cl ₂ N ₂ O ₃ ⁺		5.0
			159.9731 (6.4)	C ₆ H ₄ Cl ₂ N ⁺		5.0
TP3 	O ₂ /UVA/CAT		249.0192 (-2.2)	C ₉ H ₁₁ Cl ₂ N ₂ O ₂ ⁺		5.0
	O ₃ /UVA/CAT	10.63	159.9715 (-3.6)	C ₆ H ₄ Cl ₂ N ⁺		5.0
TP4 			244.9890 (2.21)		C ₉ H ₇ Cl ₂ N ₂ O ₂ ⁻	6.0
			216.9941 (2.56)		C ₈ H ₇ Cl ₂ N ₂ O ⁻	5.0
	O ₂ /UVA/CAT	10.42	187.9675 (2.69)		C ₇ H ₄ Cl ₂ NO ⁻	5.0
	O ₃		159.9726 (3.25)		C ₆ H ₄ Cl ₂ N ⁻	4.0
	O ₃ /UVA/CAT		58.0298 (8.80)		C ₂ H ₄ NO ⁻	
			247.0812 (1.3)	C ₉ H ₉ Cl ₂ N ₂ O ₂ ⁺		6.0
			10.45	123.9968 (11.3)	C ₆ H ₅ ClN ⁺	
DIU 			60.0444 (-8.9)	C ₂ H ₆ NO ⁺		1.0
			231.0097 (2.2)		C ₉ H ₉ Cl ₂ N ₂ O ⁻	5.0
	O ₂ /UVA/CAT	9.62	185.9519 (3.0)		C ₇ H ₂ Cl ₂ NO ⁻	5.0
	O ₃		149.9744 (-1.2)		C ₇ HClNO ⁻	5.0
	O ₃ /UVA/CAT	9.58	233.0243 (-2.3)	C ₉ H ₁₁ Cl ₂ N ₂ O ⁺		5.0
TP5 	O ₃ /UVA/CAT		187.9664 (-3.2)	C ₇ H ₄ Cl ₂ NO ⁺		5.0
			159.9715 (-3.6)	C ₆ H ₄ Cl ₂ N ⁺		4.0
			72.0444 (-7.5)	C ₃ H ₆ NO ⁺		2.0
TP5 	O ₂ /UVA/CAT	9.20	216.9941 (2.56)		C ₈ H ₇ Cl ₂ N ₂ O ⁻	5.0
	O ₃		159.9726 (3.2)		C ₆ H ₄ Cl ₂ N ⁻	4.0

	O ₃ /UVA/CAT	9.27	219.0081 (-4.9)	C ₈ H ₉ Cl ₂ N ₂ O ⁺	5.0	
			161.9869 (-5.2)	C ₆ H ₆ Cl ₂ N ⁺	4.0	
			127.0183 (-4.54)	C ₆ H ₆ ClN ⁺	4.5	
	O ₂ /UVA/CAT	6.44	213.0425 (-2.7)	C ₉ H ₁₀ ClN ₂ O ₂ ⁻	5.0	
			167.9858 (3.4)	C ₇ H ₃ ClNO ₂ ⁻	6.0	
			139.9909 (4.2)	C ₆ H ₃ ClNO ⁻	N/A	
			O ₃	132.0091 (4.1)	C ₇ H ₂ NO ₂ ⁻	N/A
			O ₃ /UVA/CAT	215.0582 (-1.1)	C ₉ H ₁₂ ClN ₂ O ₂ ⁺	5.0
	O ₃	1.44	6.59	126.9945 (-4.5)	C ₆ H ₄ ClO ⁺	4.0
			72.0440 (-13.0)	C ₃ H ₆ NO ⁺	1.0	
			203.0662 (-2.9)	C ₇ H ₁₁ N ₂ O ₅ ⁺	4.0	
			185.0566 (1.98)	C ₇ H ₉ N ₂ O ₄ ⁺	3.0	
	O ₃	1.44	157.0604 (-5.8)	C ₆ H ₉ N ₂ O ₃ ⁺	3.0	
			72.0462 (17.5)	C ₃ H ₆ NO ⁺	2.0	
			201.94681 (9.1)	C ₇ H ₂ Cl ₂ NO ₂ ⁻	6.0	
	O ₂ /UVA/CAT	9.54	165.9701 (3.12)	C ₇ HCINO ₂ ⁻	N/A	
			TP9	O ₂ /UVA/CAT	187.9675 (2.7)	C ₇ H ₄ Cl ₂ NO ⁻
	O ₃	10.44	159.9726 (3.2)	C ₆ H ₄ Cl ₂ N ⁻	4.0	
			O ₃ /UVA /CAT	116.0142 (4.8)	C ₇ H ₂ NO ⁻	N/A
	O ₂ /UVA/CAT	9.23	159.9726 (1.9)	C ₆ H ₄ Cl ₂ N ⁻	4.0	
			O ₃	123.9960 (4.8)	C ₆ H ₃ ClN ⁻	5.0
	O ₃ /UVA/CAT	9.23	123.9960 (4.8)	C ₆ H ₃ ClN ⁻	5.0	

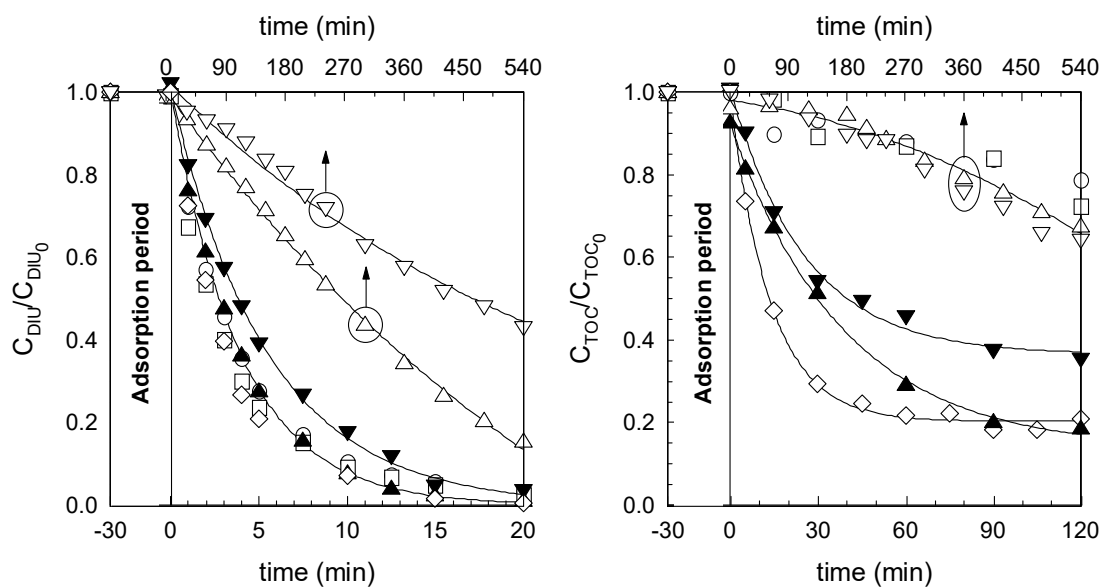


Figure 1. Normalized concentration of diuron (left) and TOC removal (right) evolution with time under diverse technologies. Experimental conditions: $V=1.0$ L; $C_{DIU,0}=10$ mg L^{-1} ; $Q_G=30$ L h^{-1} ; $C_{O_3,inlet}=10$ mg L^{-1} ; (if applied); $C_{catalyst} = 0.5$ g L^{-1} ; $pH_0=5.6-6.0$ ○, Ozoneation; □, Catalytic ozonation; ▲, Photocatalytic ozonation with N doped TiO_2 ; ▼, Photocatalytic ozonation with undoped TiO_2 ; ◇, Photocatalytic ozonation with Degussa P25 TiO_2 ; Δ, Photocatalysis with N doped TiO_2 ; ∇, Photocatalysis with undoped TiO_2 .

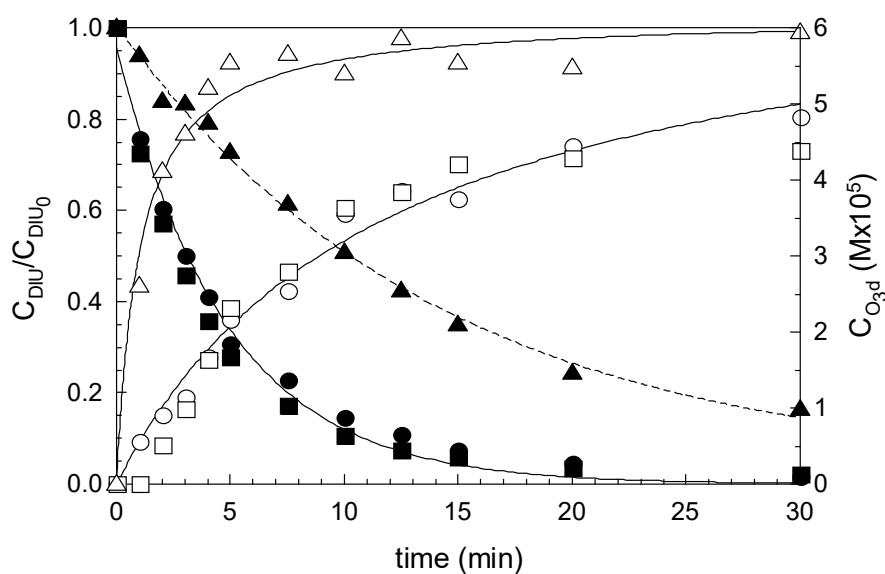


Figure 2. Ozonation of diuron. Experimental conditions: $V=1.0$ L; $Q_g=30$ L h^{-1} $C_{O_3,inlet}=10$ mg L^{-1} , $pH_0=5.6-6.0$. Ozonation: ●, $C_{DIU,0}=5$ mg L^{-1} ; ■, $C_{DIU,0}=10$ mg L^{-1} . Ozonation with tert-butyl alcohol: ▲, $C_{DIU,0}=10$ mg L^{-1} and $C_{t-BOH}=10^{-2}$ M. Empty symbols correspond to dissolved ozone concentration (C_{O_3d}). Solid lines: normalized diuron model concentration and 3rd order polynomial representing dissolved ozone. Dashed line: normalized diuron model concentration with no radical contribution.

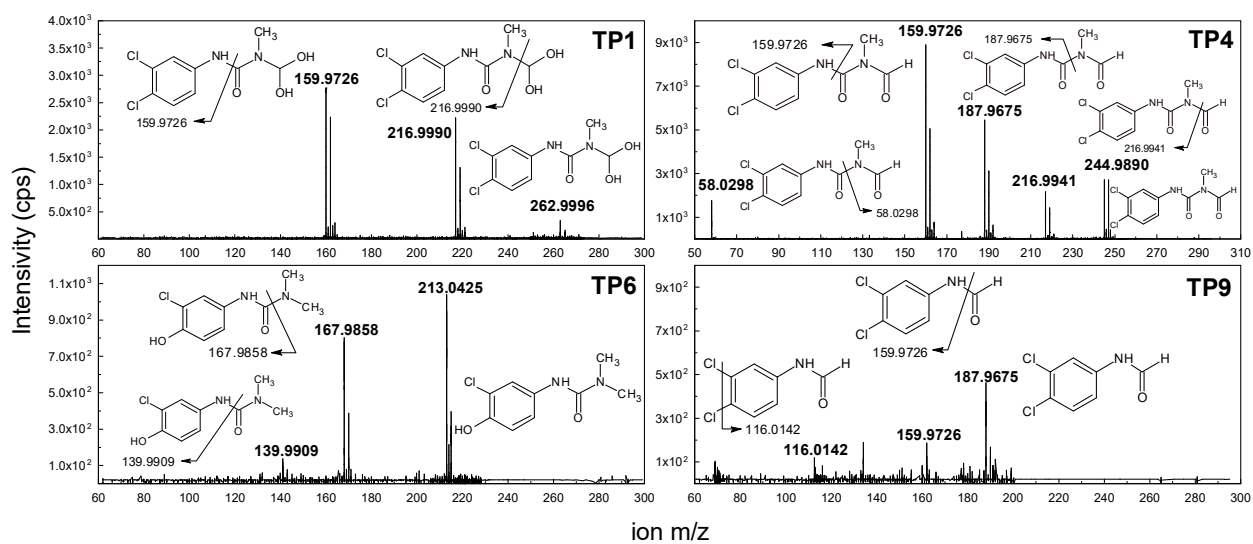


Figure 3. MS/MS fragmentation pattern spectra and fragment ion structures of some TPs found in this investigation in ESI(-)

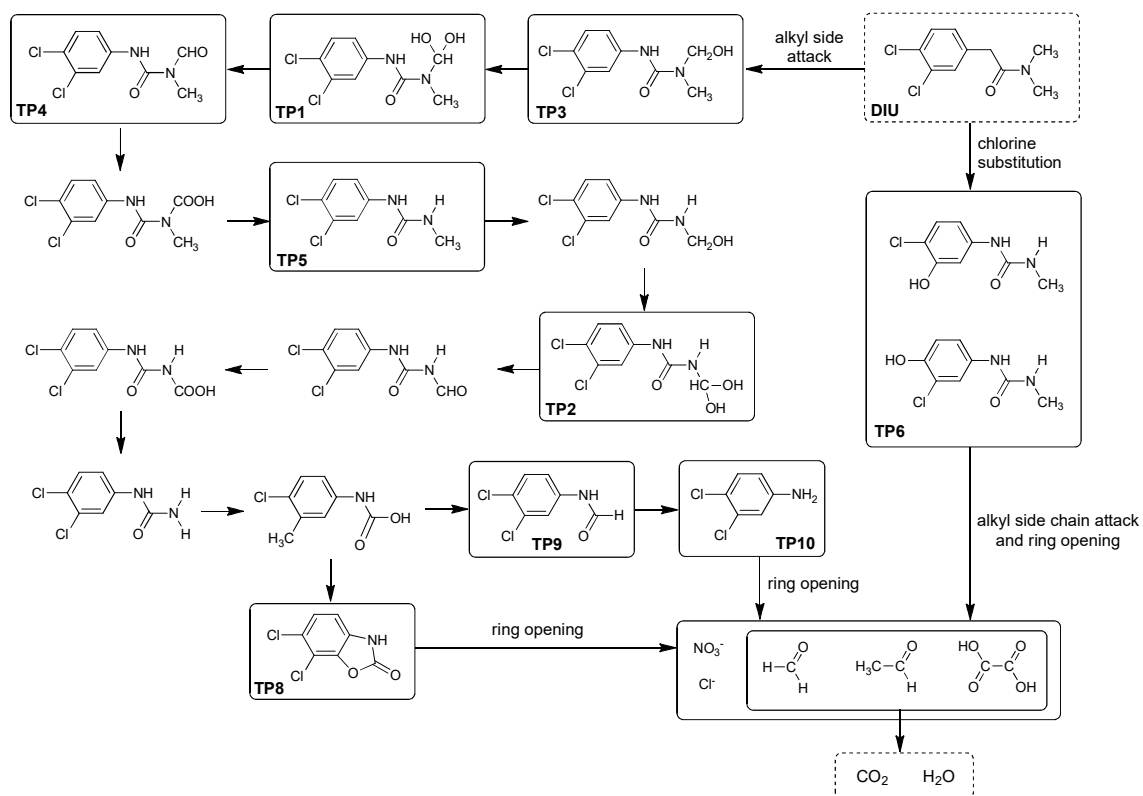


Figure 4. Tentative oxidation pathway in diuron oxidation by $\bullet\text{OH}$ radical attack. TPs detected are highlighted in boxes.

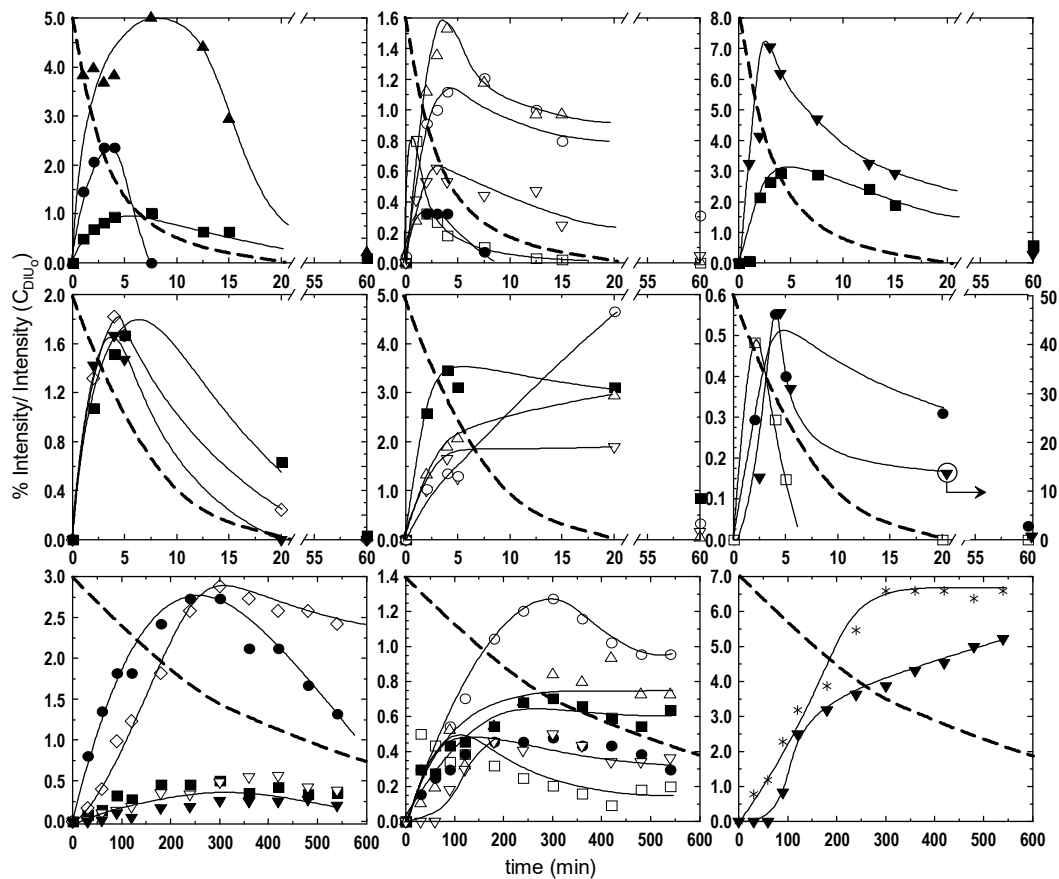


Figure 5. Evolution of normalized intensity of TPs related to maximum intensity of DIU at time zero in the ozonation (top), photocatalytic ozonation (middle) and photocatalysis (bottom) of diuron. Symbols: ∇ , TP1; \blacktriangle , TP2; \diamond , TP3; \blacktriangledown , TP4; \blacksquare , TP5; \bullet , TP6; $*$, TP8; Δ , TP9; \circ , TP10. (Dashed lines: Intensity in ESI(+) mode, solid line: Intensity in ESI(-) mode, thick dashed line: DIU evolution)

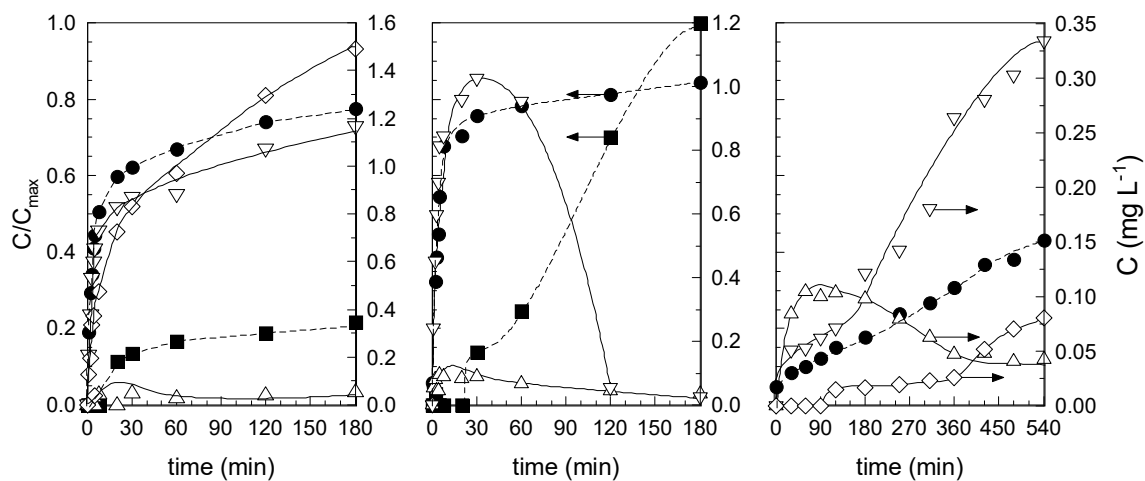


Figure 6. Anionic and short chain organic acids evolution during ozonation (left), photocatalytic ozonation (middle) and photocatalysis (right). Experimental conditions as in Figure 1. Left y-axis (dashed lines): ●, chloride normalized to maximum chloride concentration; ■, nitrate normalized to maximum nitrate concentration. Right y-axis (solid lines): Δ, acetic acid; ∇, formic acid; ◇, oxalic acid.

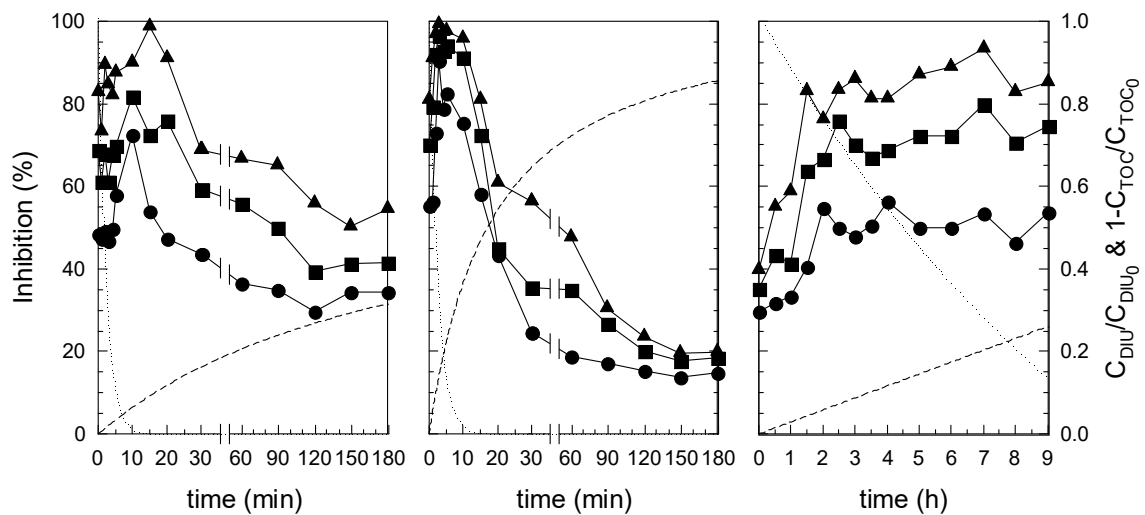


Figure 7. Toxicity evolution to *V. fischeri* during ozonation (left), photocatalytic ozonation (middle) and photocatalysis (right) at different exposure times. Experimental conditions: $V=1.0$ L; $C_{DIU,0}=10$ mg L⁻¹; $Q_G=30$ L h⁻¹; $C_{O_3inlet}=10$ mg L⁻¹; (if applied); $C_{N-TiO_2} = 0.5$ g L⁻¹; $pH_0=5.6-6.0$. Exposure time (min): ●, 5; ■, 15; ▲, 30. (Dotted lines: normalized DIU concentration, dashed lines: normalized TOC removal)